A Transient Permeation-Based Method for Composite Zeolite Membranes Characterization

L. Courthial and A. Baudot
IFP-Lyon, Direction Catalyse et Séparation, Rond-point de l'échangeur de Solaize, BP 3, 69360 Solaize, France

M. Tayakout-Fayolle
IFP-Lyon, Direction Procédés, Rond-point de l'échangeur de Solaize, BP 3, 69360 Solaize, France

C. Jallut
Université de Lyon, Université Lyon 1, Laboratoire d'Automatique et de Génie des Procédés, UMR CNRS 5007, ESCPE, 43 Bd du 11 Novembre 1918, 69622 Villeurbanne cedex France

DOI 10.1002/aic.11580
Published online September 2, 2008 in Wiley InterScience (www.interscience.wiley.com).

An in situ *nondestructive characterization method for zeolite composite membranes, based on transient permeation experiments, is proposed in the present article. This technique allows an accurate evaluation of the zeolite selective layer thickness as well as the thermodynamic and transport properties of sorbing hydrocarbons. To this end, a dynamic model representing mass transport phenomena within the whole permeating module is derived. In order to get the crystal layer properties, a two-step experimental approach is required. The zeolite layer effective thickness is first estimated with the permeation of a nonadsorbing species like hydrogen. Then, the adsorption equilibrium constants and the diffusion coefficients of butane isomers are determined. Three membranes obtained by different synthesis procedures are studied in the Henry domain. The estimated values of the equilibrium constants and diffusion coefficients for normal butane and isobutane are favorably compared with existing literature data.*
 AIChE J, 54: 2527–2538, 2008
Keywords: transient techniques, membrane, zeolite, mass transfer, dynamic modeling

Introduction

Zeolites are crystalline alumino-silicates displaying a regular and open microporous structure. Because of their intrinsic properties, such as molecular sieving and host-adsorbate interactions, zeolitic materials are often used for the separation of hydrocarbon mixtures. MFI is the most widely studied zeolite (known as ZSM-5 or the pure-silica analog, silicalite-1) for membrane application (each zeolite framework topology is designated by a three letter code, e.g. MFI, by the International Zeolite Association, www.iza-online.org). The MFI medium-sized pore network (about 0.55 nm) approaches the size of many molecules of industrial interest. Consequently, these zeolites can be used to achieve a shape-selectivity separation of alcane isomers.

An ideal composite zeolite membrane consists of a two-dimensional continuous crystal layer free of any defect, deposited on a porous support to ensure mechanical strength. The membrane zeolite layers that are used here are directly synthesized within the porous support ("pore-plugging"

Correspondence concerning this article should be addressed to C. Jallut at jallut@lagep.univ-lyon1.fr.

method). As a consequence, they can hardly be characterized by conventional nondestructive techniques. A possible solution to this problem is the use of transient state permeation experiments.

As a matter of fact, transient techniques are commonly used for the determination of transport, kinetic, and thermodynamic properties.[1] They have been used to determine solid materials heat diffusivities[2] as well as heat transfer coefficients in heat exchangers.[3,4] Inverse chromatography has been extensively used to characterize mass transfer and equilibrium properties in solid adsorbents or polymeric materials.[5–8] Inter-phase mass transfer has also been characterized dynamically in gas–liquid contactors.[9–11] Moreover, transient techniques have been used for chemical kinetics. For example, the TAP (Temporal Analysis of Product) has been used in heterogeneous catalysis[12] and for the mass transfer and equilibrium properties characterization in zeolites.[13] Impedancemetry as it is commonly used for electrochemistry is also a good example of transient approach for kinetic studies.[14] As far as membrane characterization methods are concerned, the so-called time-lag method is extensively used,[15–17] whereas Noble and coworkers[18,19] propose a transient measurement technique to characterize short ZSM-5 tubular zeolite composite membranes.

All these works are based on the application of identification techniques.[20] The properties to be determined are the parameters of the experimental set-up dynamic model. By minimizing the error between experimental and simulated data with respect to these parameters, one can get an estimation of their values.

Before the application of this approach, the structural identifiability analysis of the system model has to be made in order to determine which parameters can be theoretically estimated from the experimental input–output behavior of the system.[20] For example, such studies have been performed in the case of chromatographic columns or gas–liquid contactors.[10,21,22]

In this article, we propose a transient permeation technique for the geometrical, mass transfer, and thermodynamic characterization of composite zeolite membranes. We first describe the membrane to be characterized as well as the experimental set-up. Then, the dynamic model is presented and analyzed from a structural identifiability point of view. From this analysis, a step-by-step procedure is developed and applied to estimate the mass transport parameters through the zeolite membranes made at IFP. The main difference between our approach and the method currently described in the literature[19,23,24] is that we perform experiments in the linear domain. In this case, a simple Fick law and a linear equilibrium relation can be applied so that the parameter estimation has not to rely on detailed models for the mass transfer and equilibrium descriptions.

Structure of the Composite Membrane to be Characterized

When the so-called secondary growth (seeded) method is used, the zeolite membranes are composed of a very thin and dense zeolite layer deposited on a porous support. However, this structure is fragile due to the occurrence of voids or cracks in the crystalline phase, especially at high temperatures. The zeolite layers made at IFP are—at the opposite—grown inside the pores of a tubular support lumen. A Pall Exekia T1-70 alumina asymmetric porous tube (length 150 mm, inner diameter 6.55 mm and thickness 1.73 mm) was used as the membrane support, which is enameled at both ends for sealing purposes. One can see on Figure 1a) a SEM micrograph side view of this support. Nowadays, reproducible syntheses lead to a large amount of zeolite membranes that are available for characterization studies.

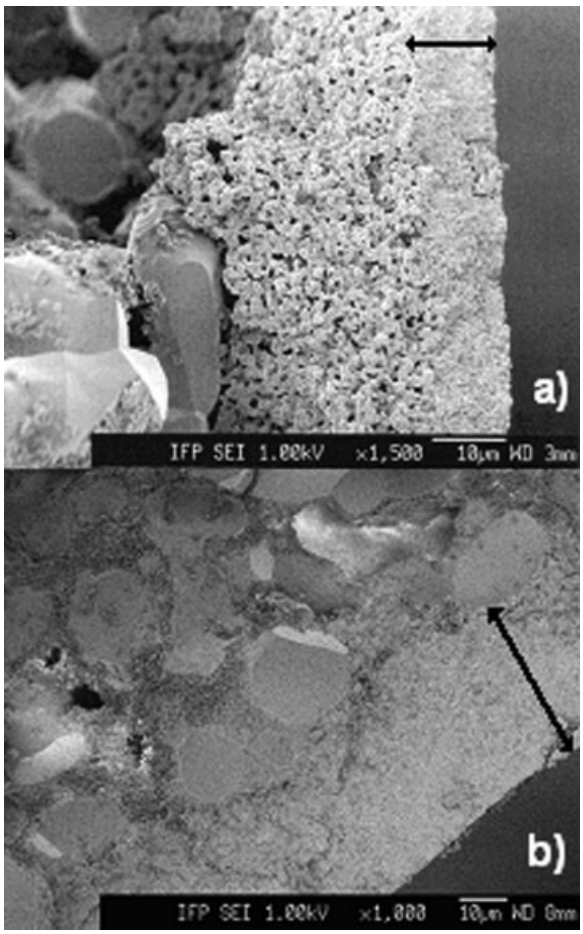

Figure 1. (a) Side view SEM micrograph of a multilayer α-Al_2O_3 Pall Exekia support: three layers of different thickness and porosity can be distinguished; (b) side view SEM micrograph of a zeolite membrane obtained by the IFP *in situ* synthesis method.

The less porous inner layer is completely filled by the zeolite crystals without any visible defects.

It is particularly of great interest to link the synthesis procedure with the zeolite layer morphological and physico–chemical properties. For instance, side view SEM can be used to measure the crystal layer thickness, but this technique has two main drawbacks: the sample has to be destroyed and the information is only local. On the contrary, the method that we propose enables a complete nondestructive characterization of the zeolite composite membranes properties. To this end, we perform the estimation of the

adsorption equilibrium constants, the diffusivities, and the average effective thickness of the zeolite selective layers.

In this study, transient experiments are performed by using *n*-butane and isobutane as sorbing hydrocarbons. Three composite membranes, respectively named M1, M2, and M3, are characterized. The synthesis procedure of these membranes is described elsewhere.[25–27] The tetrapropylammonium hydroxide (TPAOH) and silica concentrations were three times higher for the M2 and M3 syntheses ($1SiO_2$/0.4TPAOH/$63.7H_2O$) than for that of M1 ($1SiO_2$/0.4TPAOH/$18.3H_2O$). The duration and temperature of the synthesis step are the same (respectively 20 h and 175°C) as well as the calcination temperature (520°C) and duration (20 h). Figure 1b is a side view SEM of a membrane synthesized by the same procedure as M1.

Experimental Set-Up

The experimental technique that we propose is similar to the transient version of the well-known Wicke-Kallenbach diffusion cell.[28] This approach has been widely used to characterize mass transfer through porous media like catalyst pellets,[29–34] membranes, or zeolite crystals.[35,36] The principle of the transient experiments that we perform[37,38] is represented in Figure 2. A pure carrier gas initially flows through the outer and inner compartments of the module so that thermodynamic equilibrium is reached within the system. Then, the inlet composition of the inner compartment feed gas is suddenly modified according to a *n*-butane or isobutane concentration pulse injection (the input) and the two outlet compositions time evolutions (the outputs) are measured. In order to ensure that the experiments are performed in the linear domain, the linearity of the concentration responses with respect to the input intensity is verified.

The membrane to be tested is placed in a chromatograph oven (HP 5890 Series II) wherein the temperature is regulated (see Figure 3a). The set-up is operated at atmospheric pressure. Nitrogen is used as a carrier gas and its available flow rate range is comprised between 0.2 $cm^3\ s^{-1}$ and 4 $cm^3\ s^{-1}$. The gas to be injected is obtained by dilution with nitrogen through another circuit connected to the valve of the chromatograph. In order to produce the short Dirac-like concentration pulse, a controlled very short-time valve switch is produced between permeating gas tubing and sweeping gas tubing. Both outlet responses are measured by thermal conductivity detectors (TCD). Calibration curves were established in order to transform the measured signals into concentration responses.

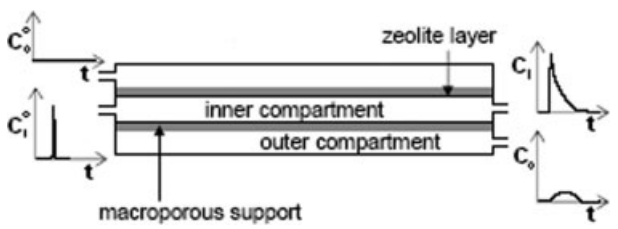

Figure 2. Transient experiments principle.

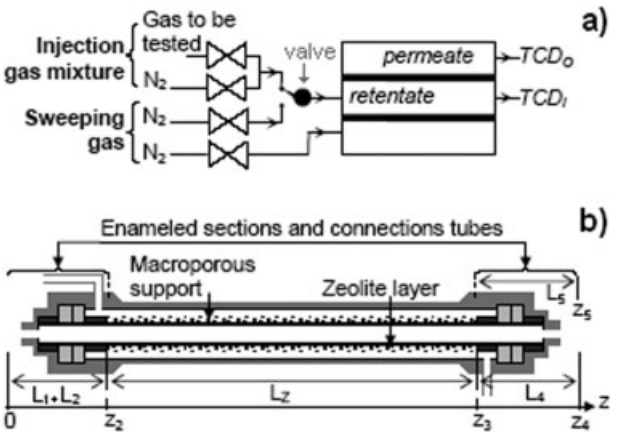

Figure 3. (a) Experimental set-up view; (b) detail of the membrane design.

By varying the initial equilibrium composition of the carrier gas, the transport and thermodynamic properties of the active zeolite layer can be studied according to its loading. In the present article, only the case of one-adsorbate experiments at zero loading will be considered. Thus, the properties that will be determined correspond to the Henry domain of the equilibrium curve.

Dynamic Modeling of the System in the Case of One-Adsorbate Permeation Experiments

The model described in this section is used to perform the simulations required for the parameters estimation procedure. The dynamic behavior of the composite membrane, the connection tubes situated between the injection devices, the TCD, and the separation module have to be represented. To this end, the permeating module is divided into three sections according to the Figure 3b. A thin part of the macroporous support contains the zeolite layer and it is enameled at both ends. As far as the system is used in the linear domain, the following assumptions are made:

- the gas phase concentrations are assumed to depend only on the axial coordinate z;
- the concentration in the zeolite layer at a given axial coordinate is assumed to depend on the radial coordinate r only;
- the flows within the compartments are represented by the plug flow and axial dispersion model;
- the zeolite layer surface and the inner compartment gas phase are assumed to be at equilibrium at a given axial coordinate;
- the adsorbate diffusion through the zeolite layer is represented by the Fick law;
- diffusive gaseous transport occurs in the macroporous support: this process is represented by lumping the adsorbate concentration profile within the macropores and by introducing the global mass transfer coefficient k_s;
- mass transfer between the outer compartment gas flow and the porous support surface is represented by the mass transfer coefficient k_o;
- all the parameters included in the model are assumed to be constant as well as the gases velocities v_i and v_o.

The zeolite layer adsorbate composition is not represented by the concentration $q(t,\eta)$ but by the following quantity:

$$C^*(t,\eta) = \frac{q(t,\eta)}{\kappa_A} \tag{1}$$

where η is the dimensionless radial coordinate. This choice of state variable for the zeolite layer composition will be justified by the structural identifiability analysis that is performed in the following section. Firstly, let us consider the zone containing the zeolite layer (see Figure 3b). The dimensionless adsorbate material balances in the inner and outer compartments are as follows:

$$\begin{cases} z_2 < z < z_3 \\ \dfrac{\partial C_i}{\partial t} = -\dfrac{1}{\tau_i^{L_z}}\dfrac{\partial C_i}{\partial \xi} + \dfrac{1}{\tau_i^{L_z} Pe_i^{L_z}}\dfrac{\partial^2 C_i}{\partial \xi^2} + a_i B_z \dfrac{\partial C^*(t,\eta=0)}{\partial \eta} \\ \dfrac{\partial C_o}{\partial t} = -\dfrac{1}{\tau_o^{L_z}}\dfrac{\partial C_o}{\partial \xi} + \dfrac{1}{\tau_o^{L_z} Pe_o^{L_z}}\dfrac{\partial^2 C_o}{\partial \xi^2} - \varepsilon a_o k_o (C_o - C_s) \end{cases} \tag{2}$$

$C^*(t,\eta = 0)$ is the concentration of the gas phase in contact with the zeolite layer inner surface. $B_z = \frac{\kappa_A D_z}{e_z}$ is a mass transfer parameter involved in the boundary condition of the zeolite layer inner surface. According to the state variable given by Eq. 1, the adsorbate material balance in the zeolite layer is:

$$\begin{cases} z_2 < z < z_3 \\ \frac{\partial C^*}{\partial t} = \frac{1}{\tau_z}\left(\frac{\partial^2 C^*}{\partial \eta^2} + \frac{1}{\eta}\frac{\partial C^*}{\partial \eta}\right) \end{cases} \tag{3}$$

where $\tau_z = e_z^2/D_z$ is the diffusion time constant. The adsorbate mass balance in the porous support is given by:

$$\begin{cases} z_2 < z < z_3 \\ \frac{\partial C_s}{\partial t} = -a_z k_s (C_s - C^*(t,\eta=1)) + a_o k_o (C_o - C_s) \end{cases} \tag{4}$$

$C^*(t,\eta = 1)$ is the concentration of the gas phase in contact with the zeolite layer outer surface. Let us now consider the zones that do not contain the zeolite layer. The flows associated to the enameled zones of the support as well as a part of the connection tubes are represented by the Plug flow—Axial dispersion model (designated by the P-D model) according to the following equations (see Figure 4):

$$\begin{cases} z_1 < z < z_2 \\ \dfrac{\partial C_i^2}{\partial t} = -\dfrac{1}{\tau_i^{L_2}}\dfrac{\partial C_i^2}{\partial \xi_2} + \dfrac{1}{\tau_i^{L_2} Pe_i^{L_2}}\dfrac{\partial^2 C_i^2}{\partial \xi_2^2} \end{cases}$$
$$\begin{cases} z_3 < z < z_4 \\ \dfrac{\partial C_i^4}{\partial t} = -\dfrac{1}{\tau_i^{L_4}}\dfrac{\partial C_i^4}{\partial \xi_4} + \dfrac{1}{\tau_i^{L_4} Pe_i^{L_4}}\dfrac{\partial^2 C_i^4}{\partial \xi_4^2} \\ z_3 < z < z_5 \\ \dfrac{\partial C_o^5}{\partial t} = -\dfrac{1}{\tau_o^{L_5}}\dfrac{\partial C_o^5}{\partial \xi_5} + \dfrac{1}{\tau_o^{L_5} Pe_o^{L_5}}\dfrac{\partial^2 C_o^5}{\partial \xi_5^2} \end{cases} \tag{5}$$

The boundary conditions between these sub-models are defined at the inlets and outlets of each flow section as well as at the membrane surfaces (zeolite layer and alumina support):

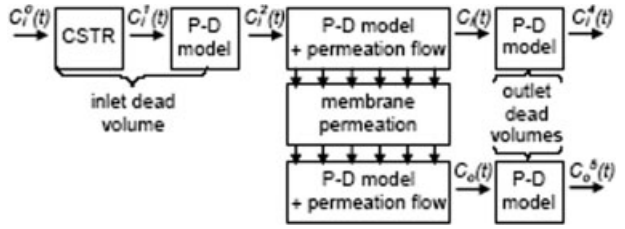

Figure 4. Flow model of the experimental set-up.

$$\left.\begin{array}{l} \text{Zeolite layer surfaces :} \\ \begin{cases} z_2 < z < z_3 \\ C^*(t,\xi,\eta=0) = C_i(t,\xi) \\ B_z \frac{\partial C^*(t,\xi,\eta=1)}{\partial \eta} = \varepsilon k_s (C_s(t,\xi) - C^*(t,\xi,\eta=1)) \end{cases} \\ \text{Flows inlets :} \\ \begin{cases} C_i(t,\xi=0) = C_i^2(t,\xi_2=1), \quad C_i^4(t,\xi_4=0) = C_i(t,\xi=1) \\ C_o(t,\xi=0) = 0, \qquad C_o^5(t,\xi_5=0) = C_o(t,\xi=1) \end{cases} \\ \text{Flow outlets :} \\ \begin{cases} \frac{\partial C_i^2}{\partial \xi_2}(t,\xi_2=1) = 0, \quad \frac{\partial C_i}{\partial \xi}(t,\xi=1) = 0, \quad \frac{\partial C_i^4}{\partial \xi_4}(t,\xi_4=1) = 0 \\ \qquad\qquad \frac{\partial C_o}{\partial \xi}(t,\xi=1) = 0, \quad \frac{\partial C_o^5}{\partial \xi_5}(t,\xi_5=1) = 0 \end{cases} \end{array}\right\} \tag{6}$$

Finally, to complete the description of the tubes connected to the inner compartment, a CSTR has turned to be necessary according to the following balance equation and boundary condition (see Figure 4):

$$\begin{cases} 0 < z < z_1 \\ \frac{dC_i^1}{dt} = \frac{1}{\tau_i^{CSTR}}(C_i^0 - C_i^1) \\ C_i^2(t,\xi_2=0) = C_i^1(t) \end{cases} \tag{7}$$

An implicit finite difference scheme is used for the model simulation and the parameters estimation is obtained with the Levenberg-Marquardt algorithm. The code is written with the Fortran® language and the IMSL® library BCLSF algorithm is used for the optimization.

Structural Identifiability Analysis

Introduction

The simulation model exhibits a great number of parameters. Only those related to the zeolite layer are of interest: the diffusion coefficient D_z, the equilibrium constant κ_A, and the layer thickness e_z. From that point, one has to address a very important question: can these three parameters D_z, κ_A, and e_z be obtained independently from the input–output behavior of the system? The objective of the structural identifiability analysis is to answer this question and to propose an experimental step-by-step strategy to get all the relevant parameters corresponding to the zeolite layer properties.

Within the framework of chromatographic studies,[21,22] it has been shown that the stagnant phase composition should not be represented by the adsorbate concentration q. Indeed, it is necessary to use the adsorbate concentration C^* in a gas phase that would be at equilibrium with the solid phase. This change of state variable avoids any over-parameterization of the model. To validate the change of the state variable given

by Eq. 1 in the case of the membrane model, the structural identifiability analysis is realized with the transfer function technique.[20,22] In order to simplify the transfer functions derivation, we use a simplified version of the model where the gas phase axial dispersions are neglected, the selective layer curvature is not taken into account and the support is not considered. Because the result is totally based on the way the adsorbent composition in the zeolite is represented, these simplifications will not change the main conclusion of the structural study of the model.

The simplified model

The adsorbate balance equations and boundary conditions for the inner and outer compartments become:

$$\begin{cases} \text{Balance equation :} \\ \frac{\partial C_\mathrm{i}}{\partial t} = -\frac{1}{\tau_\mathrm{i}^{\mathrm{L_z}}}\frac{\partial C_\mathrm{i}}{\partial \xi} + a_\mathrm{i}B_\mathrm{z}\frac{\partial C^*(t,\eta=0)}{\partial \eta} \\ \frac{\partial C_\mathrm{o}}{\partial t} = -\frac{1}{\tau_\mathrm{o}^{\mathrm{L_z}}}\frac{\partial C_\mathrm{o}}{\partial \xi} - a_\mathrm{o}k_\mathrm{o}(C_\mathrm{o} - C^*(t,\eta=1)) \\ \text{Boundary conditions :} \\ C_\mathrm{i}(t,\xi=0) = C_\mathrm{i}^0(t) \\ C_\mathrm{o}(t,\xi=0) = 0 \end{cases} \tag{8}$$

where $C_\mathrm{i}^0(t)$ is the inner compartment gas phase inlet concentration. The zeolite layer adsorbate balance equation and the associated boundary conditions are as follows:

$$\begin{cases} \text{Mass balance equation in the zeolite layer :} \\ \frac{\partial C^*}{\partial t} = \frac{1}{\tau_\mathrm{z}}\left(\frac{\partial^2 C^*}{\partial \eta^2}\right) \\ \text{Boundary conditions :} \\ C^*(t,\eta=0) = C_\mathrm{i} \\ \frac{\partial C^*}{\partial \eta}(t,\eta=1) = \frac{k_\mathrm{o}}{B_\mathrm{z}}(C_\mathrm{o} - C^*(t,\eta=1)) \end{cases} \tag{9}$$

$\frac{k_\mathrm{o}}{B_\mathrm{z}} = \frac{k_\mathrm{o}e_\mathrm{z}}{\kappa_\mathrm{A}D_\mathrm{z}}$ is a dimensionless Biot number including the equilibrium constant involved in the boundary conditions between the zeolite layer surface and the outer compartment.

Structural identifiability analysis of the simplified model

For the sake of the presentation simplification, only the transfer function between the inner compartment inlet concentration and the outer compartment outlet concentration is derived: $G(s) = \hat{C}_\mathrm{o}(s,\xi=1)/\hat{C}_\mathrm{i}(s,\xi=0)$. Only the main steps of this long and tedious derivation are detailed. The system is assumed to be initially at equilibrium so that the initial conditions are null. The Laplace transforms of Eqs. 8 and 9 are as follows:

$$\begin{cases} \frac{1}{\tau_\mathrm{i}^{\mathrm{L_z}}}\frac{\partial \hat{C}_\mathrm{i}}{\partial \xi} + s\hat{C}_\mathrm{i} - a_\mathrm{i}B_\mathrm{z}\frac{\partial \hat{C}^*(\eta=0)}{\partial \eta} = 0 \\ \frac{1}{\tau_\mathrm{o}^{\mathrm{L_z}}}\frac{\partial C_\mathrm{o}}{\partial \xi} + s\hat{C}_\mathrm{o} + k_\mathrm{o}a_\mathrm{o}\left(\hat{C}_\mathrm{o} - \hat{C}^*(\eta=1)\right) = 0 \\ C_\mathrm{i}(s,\xi=0) = \hat{C}_\mathrm{i}^0(s) \\ \hat{C}_\mathrm{o}(s,\xi=0) = \hat{C}_\mathrm{o}^0(s) = 0 \end{cases} \tag{10}$$

$$\begin{cases} s\hat{C}^* = \frac{1}{\tau_\mathrm{z}}\frac{\partial^2 \hat{C}^*}{\partial \eta^2} \\ \hat{C}^*(\eta=0) = \hat{C}_\mathrm{i} \\ \frac{\partial \hat{C}^*(\eta=1)}{\partial \eta} = \frac{k_\mathrm{o}}{B_\mathrm{z}}\left(\hat{C}_\mathrm{o} - \hat{C}^*(\eta=1)\right) \end{cases} \tag{11}$$

Equation 11 are solved with respect to η so that one can express $\hat{C}^*(\eta=0)$ and $\hat{C}^*(\eta=1)$ as functions of $\hat{C}_\mathrm{i}$ and $\hat{C}_\mathrm{o}$. By including these results into Eq. 10 and solving them with respect to ξ, one finally finds the transfer function $G(s) = \hat{C}_\mathrm{o}(s,\xi=1)/\hat{C}_\mathrm{i}(s,\xi=0)$. The following intermediate expressions are obtained for the zeolite layer:

$$\hat{C}^*(s,\eta) = a_1(s)e^{\eta\sqrt{\tau_\mathrm{z}s}} + a_2(s)e^{-\eta\sqrt{\tau_\mathrm{z}s}} \tag{12}$$

with

$$\begin{aligned} a_1(s) &= \frac{-\hat{C}_\mathrm{i}(1-l_\mathrm{o})e^{-\sqrt{\tau_\mathrm{z}s}} + \hat{C}_\mathrm{o}}{(1+l_\mathrm{o})e^{\sqrt{\tau_\mathrm{z}s}} - (1-l_\mathrm{o})e^{-\sqrt{\tau_\mathrm{z}s}}} \\ a_2(s) &= \frac{\hat{C}_\mathrm{i}(1+l_\mathrm{o})e^{\sqrt{\tau_\mathrm{z}s}} - \hat{C}_\mathrm{o}}{(1+l_\mathrm{o})e^{\sqrt{\tau_\mathrm{z}s}} - (1-l_\mathrm{o})e^{-\sqrt{\tau_\mathrm{z}s}}} \\ l_\mathrm{o}(s) &= \frac{B_\mathrm{z}}{k_\mathrm{o}}\sqrt{\tau_\mathrm{z}s} \end{aligned}$$

The boundary conditions can be expressed with the following expressions:

$$\begin{aligned} \frac{\partial C^*(\eta=0)}{\partial \eta} &= 2\sqrt{\tau_\mathrm{z}s}\frac{-\hat{C}_\mathrm{i} + \hat{C}_\mathrm{o}}{(1+l_\mathrm{o})e^{\sqrt{\tau_\mathrm{z}s}} - (1-l_\mathrm{o})e^{-\sqrt{\tau_\mathrm{z}s}}} \\ C^*(\eta=1) &= \frac{2l_\mathrm{o}\hat{C}_\mathrm{i} + \left(e^{\sqrt{\tau_\mathrm{z}s}} - e^{-\sqrt{\tau_\mathrm{z}s}}\right)\hat{C}_\mathrm{o}}{(1+l_\mathrm{o})e^{\sqrt{\tau_\mathrm{z}s}} - (1-l_\mathrm{o})e^{-\sqrt{\tau_\mathrm{z}s}}} \end{aligned} \tag{13}$$

By including Eq. 13 into 10, one finally finds the transfer function:

$$G(s) = \frac{D(s)}{r_1(s) - r_2(s)}\left(e^{r_1(s)} - e^{r_2(s)}\right) \tag{14}$$

with

$$\begin{aligned} \Delta(s) &= (A(s) - C(s))^2 + 4B(s)D(s) \\ r_1(s) &= \frac{-(A(s)+C(s)) + \sqrt{\Delta(s)}}{2} \\ r_2(s) &= \frac{-(A(s)+C(s)) - \sqrt{\Delta(s)}}{2} \end{aligned} \tag{15}$$

$$\begin{aligned} A(s) &= \tau_\mathrm{i}^{\mathrm{L_z}}\left(s + 2a_\mathrm{i}B_\mathrm{z}\frac{\sqrt{\tau_\mathrm{z}s}}{(1+l_\mathrm{o})e^{\sqrt{\tau_\mathrm{z}s}} - (1-l_\mathrm{o})e^{-\sqrt{\tau_\mathrm{z}s}}}\right) \\ B(s) &= 2\tau_\mathrm{i}^{\mathrm{L_z}}a_\mathrm{i}B_\mathrm{z}\frac{\sqrt{\tau_\mathrm{z}s}}{(1+l_\mathrm{o})e^{\sqrt{\tau_\mathrm{z}s}} - (1-l_\mathrm{o})e^{-\sqrt{\tau_\mathrm{z}s}}} \\ C(s) &= \tau_\mathrm{o}^{\mathrm{L_z}}\left(s + a_\mathrm{o}k_\mathrm{o}\left(1 - \frac{\left(e^{\sqrt{\tau_\mathrm{z}s}} - e^{-\sqrt{\tau_\mathrm{z}s}}\right)}{(1+l_\mathrm{o})e^{\sqrt{\tau_\mathrm{z}s}} - (1-l_\mathrm{o})e^{-\sqrt{\tau_\mathrm{z}s}}}\right)\right) \\ D(s) &= 2\tau_\mathrm{o}^{\mathrm{L_z}}a_\mathrm{o}k_\mathrm{o}\frac{l_\mathrm{o}}{(1+l_\mathrm{o})e^{\sqrt{\tau_\mathrm{z}s}} - (1-l_\mathrm{o})e^{-\sqrt{\tau_\mathrm{z}s}}} \end{aligned} \tag{16}$$

From the transfer function expression, we deduce that the dynamic input–output behavior of the simplified model only depends on the following macroparameters or groups of parameters[20]: $\tau_\mathrm{i}^{\mathrm{L_z}}, \tau_\mathrm{o}^{\mathrm{L_z}}, \tau_\mathrm{z}, a_\mathrm{i}B_\mathrm{z}, a_\mathrm{o}k_\mathrm{o}, \frac{B_\mathrm{z}}{k_\mathrm{o}}$. A similar conclusion would have been drawn from the calculation of the second transfer function $H(s) = \hat{C}_\mathrm{i}(s,\xi=1)/\hat{C}_\mathrm{i}(s,\xi=0)$. Only two macroparameters include the zeolite layer properties:

$\tau_z = e_z^2/D_z$ and $B_z = \kappa_A D_z/e_z$. Consequently, even if τ_z and B_z are well estimated, it is impossible to determine, respectively, κ_A, D_z, and e_z. A step-by-step experimental characterization strategy similar to the one described elsewhere[17] is then proposed. By using an adsorbate whose adsorption constant κ_A is known or an inert component for which we can assume that $\kappa_A \approx 1$, the selective layer thickness e_z can be estimated. This first result can be validated by comparing the estimations of e_z and D_z to the expected orders of magnitude. Because e_z is constant, when an adsorbate of interest is used, one can estimate D_z and κ_A for this species. According to our step-by-step approach, the other parameters of the model (axial dispersion coefficients, mass transfer coefficients) are also determined from specific experiments that are described in the following sections.

Inner and Outer Compartments Flows Modeling

The flow patterns had to be characterized before be used for the zeolite layer characterization. To this end, the composite membrane was replaced by a nonporous stainless steel tube having strictly similar dimensions, and hydrogen was used as a tracer. Fourteen volumetric flow rates regularly distributed between 0.2 $cm^3\ s^{-1}$ and 4.0 $cm^3\ s^{-1}$ have been tested according to the three operating temperatures (23°C, 100°C, and 200°C). The Reynolds numbers based on the hydraulic diameter d_H are comprised between 0.3 and 5.1 so that the flow regime is laminar. The model representing the tracer transport through both the inner and outer compartments is given by Eq. 2 where the fluxes between the gas flows and the tube wall are equal to zero. According to the new geometry due to the use of a stainless steel tube, one has to consider the total lengths $L_{t,i} = L_2 + L_z + L_4$ and $L_{t,o} = L_2 + L_z + L_5$ associated to the inner and outer plug and

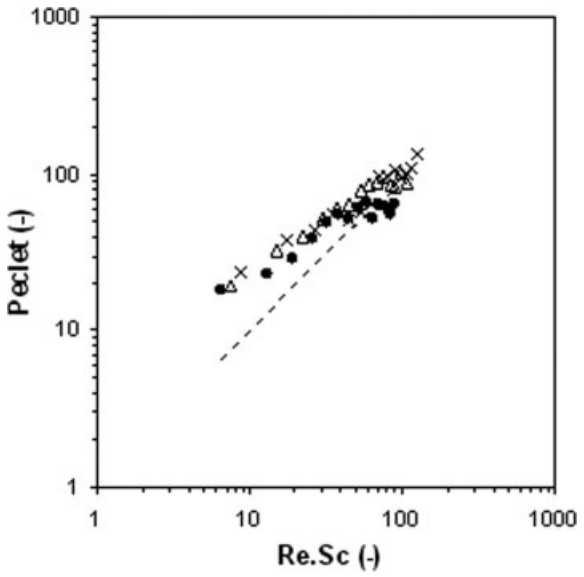

Figure 5. Inner compartment Peclet number as a function of *ReSc*.

Dashed lines: values estimated with Aris theory, ● 200°C, △ 100°C, × 21.5°C.

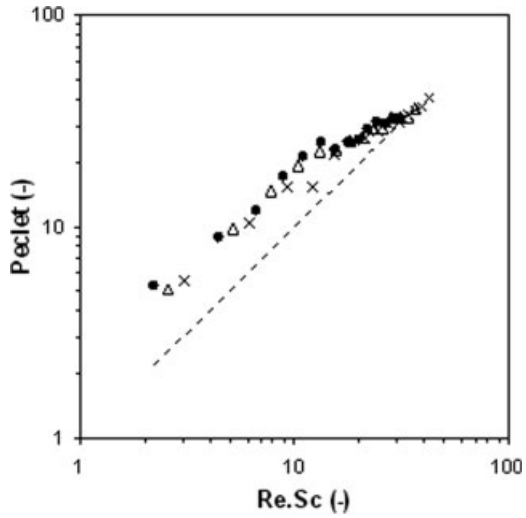

Figure 6. Outer compartment Peclet number as a function of *ReSc*.

Dashed lines: values estimated with Aris theory, ● 200°C, △ 100°C, × 21.5°C.

axially dispersed flows. The estimation procedure is then applied to the corresponding Peclet numbers $Pe_i^{L_{t,i}}$ and $Pe_o^{L_{t,o}}$ as well as to the CSTR volume. This CSTR is used to represent a supplementary mixing process due to the set-up tubing and the injection valve (see Figure 4). The estimated Peclet numbers are presented as a function of the dimensionless number *Re Sc*. Hydrogen molecular diffusion coefficient D_m is obtained thanks to the Wilke and Lee relation, whereas the gas phase viscosity is calculated by using the Chung et al. method.[39] One can see on the Figures 5 and 6 that the Peclet and the *Re Sc* numbers are closely correlated for both the inner and the outer compartments. We have also compared the experimental results with those given by Aris[40] for the axial dispersion coefficient:

$$D_{ax} = D_m + d_H^2 v^2 / 192 D_m \tag{17}$$

A good accordance between our results and Aris model is observed (see Figures 5 and 6). Aris approach was developed for flows in pipes having a circular cross section. Possible entry hydrodynamic effects can explain the slight deviation between the experimental and the calculated results. The volume of the CSTR that is used to represent the mixing process at the inner compartment inlet is not sensitive to the operating conditions. The estimated value of V^{CSTR} is 0.8 ml that represents about 9% of the total inner circuit volume.

Zeolite Layer Effective Thickness Estimation

Hydrogen was used as a nonadsorbing tracer and its adsorption coefficient κ_A is assumed to be equal to 1.[38] In order to check that the estimated effective zeolite layer thickness is not sensitive to operating conditions, transient permeation measurements were performed for different temperatures (23°C, 100°C, and 200°C) and flow rates (0.278, 1.11, and 1.94 $Ncm^3\ s^{-1}$) on the M1 membrane: Figure 7 is an

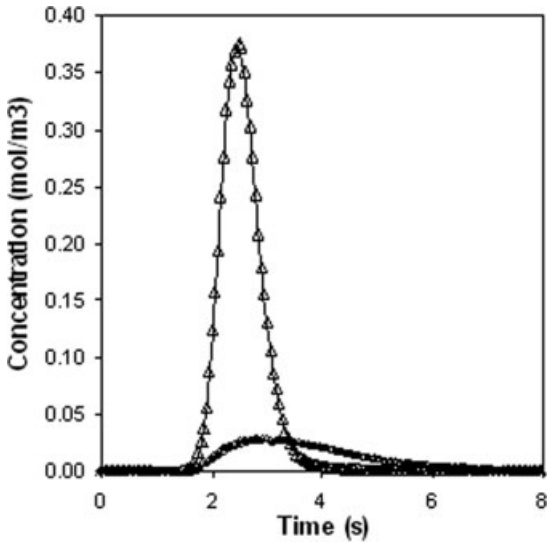

Figure 7. Example of outlet hydrogen concentration evolutions (membrane: M1, temperature: 200°C, volumetric inner and outer compartment flow rates: 3.40 $cm^3\ s^{-1}$).

Solid lines: model simulation, Δ: experimental values for the inner compartment, ○: experimental values for the outer compartment.

example of model fitting. The M1 membrane effective thickness has been estimated to $e_z = 26\ \mu m$. The membranes M2 and M3 are supposed to be strictly identical due to their synthesis procedure. Consequently, their thicknesses are assumed to be equal and only the one of the M2 membrane has been estimated to $e_z = 9\ \mu m$.

The estimated hydrogen diffusion coefficients within the zeolite layers are shown in the Figure 8 and compared with literature data. The diffusivity obtained with a macroscopic technique applied to a metal-supported silicalite-1 zeolite membrane is close to our transient permeation measurements results.[43] The hydrogen diffusion coefficient obtained by considering a Maxwell-Stefan diffusion process including only surface diffusion is slightly different than our estimation.[41] This can be due to the differences in the zeolite membranes structures that have not been synthesized by the same technique. The order of magnitude of these results is comparable and the experimental results for the M1 membrane show a coherent hydrogen diffusivity increase with temperature. The transient permeation measurements technique can thus be used to reliably characterize zeolite membranes effective thicknesses.

Let us notice that the hydrogen diffusion coefficient in membrane M1 is significantly higher than in membrane M2. Possible defects between crystals that are more likely to occur in thinner membranes, can explain this difference. Another explanation could rely on a higher occurrence of crystal intergrowth effects in the thicker membrane leading to enhanced pore network heterogeneities throughout the permeating species diffusion path. These possible intra-crystalline transport barriers could lead to a hindrance of diffusion through the thicker layer.[42]

Analysis of Additional Mass Transport Resistances

The transient experiments performed with hydrogen have also been used to check for the influence of the mass transfer processes through the porous support. On one hand, the mass transfer resistance within the macroporous support has been found negligible. On the other hand, the mass transfer coefficient k_o has been found to be sensitive. The estimated value of k_o has been compared with two mass transfer correlations available in the literature:

$$Sh = 1.614\ \phi(\alpha)\left(\frac{d_H}{L}\right)^{1/3} Re_{d_H} Sc$$
$$\phi(\alpha) = \frac{(1-\alpha)}{\alpha}\left[\frac{0.5 - \frac{\alpha^2}{(1-\alpha^2)}\ln\left(\frac{1}{\alpha}\right)}{\frac{(1+\alpha^2)}{(1-\alpha^2)}\ln\left(\frac{1}{\alpha}\right) - 1}\right] \quad (18)$$

where $\alpha = \frac{\text{inner diameter of the annuli}}{\text{outer diameter of the annuli}}$ and $Sh = \frac{k_o d_H}{D_m}$

$$Sh = 0.644\left(\frac{d_H}{L}\right)^{1/2} Re_{d_H}^{1/2} Sc^{1/2} \quad (19)$$

As far as the geometry of our system is concerned, Eq. 18 seems to be the most suitable for the outer compartment because it is adapted to fully developed laminar flow through annulus ducts.[44] On the contrary, Eq. 19 was obtained for laminar flows inside a tube[45] and is more relevant for the hydrodynamic conditions on the retentate side. Thus, for the permeate compartment, this correlation was adapted by using the hydraulic diameter.

One can see on Figure 9 that the values of k_o obtained by the transient permeation method increase with the volumetric flow rate and in a less extent with the temperature. The correlations (18) and (19) lead to values distributed according to

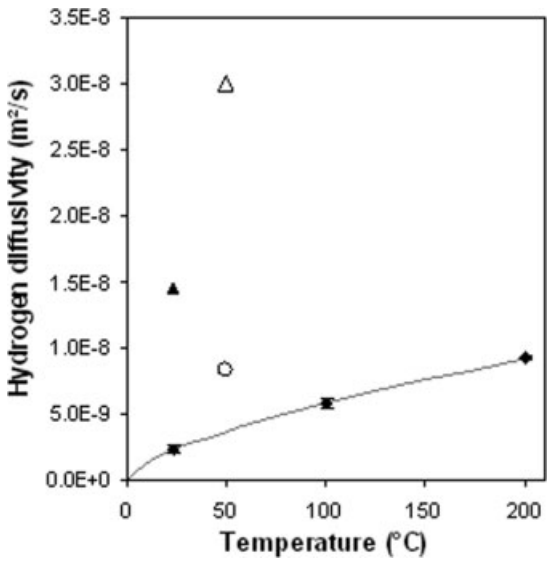

Figure 8. Hydrogen diffusion coefficients in the zeolite layer as a function of temperature.

Present work: ♦ membrane M1 and ▲ membrane M2, ○ Bakker[43], Δ Ciavarella[41].

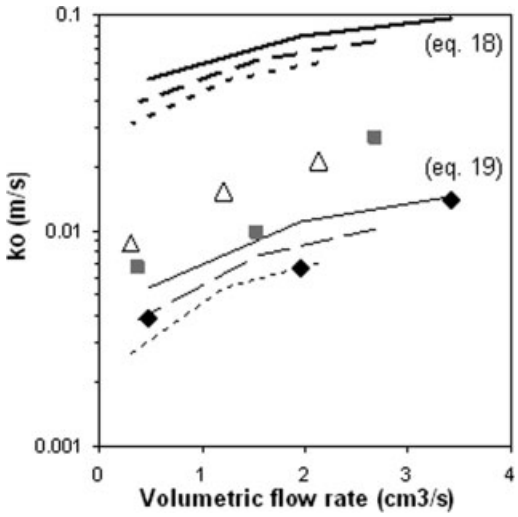

Figure 9. Hydrogen mass transfer coefficient k_o in M1 as a function of the volumetric flow rate.

♦ 200°C, ■ 100°C, △ 21.5°C. Results given by correlations (solid lines: 200°C; dashed lines: 100°C; doted lines: 21.5°C).

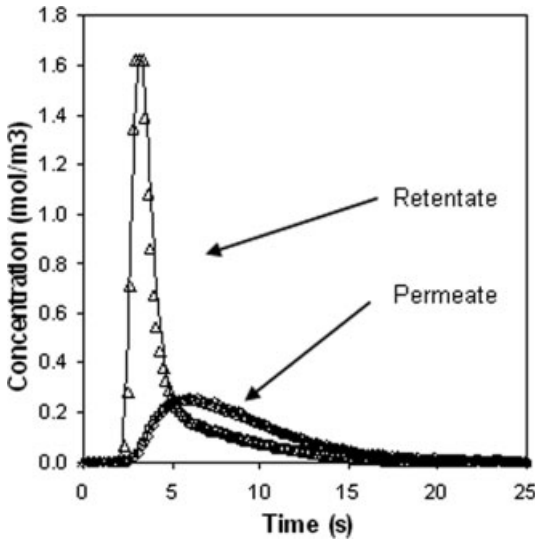

Figure 11. Example of outlet normal butane concentration evolutions (membrane: M1, temperature 200°C, volumetric inner and outer compartment flow rates: 3.0 cm^3 s^{-1}).

Solid lines: model simulation; △: experimental values for the inner compartment, ○: experimental values for the outer compartment.

two orders of magnitude but the evolutions vs. flow rate and temperature are in a relatively good accordance with the whole data. This comparison can be considered as a satisfying result if one considers the unknown entry hydrodynamic effects in the outer compartment. The observation of Figure 9 tends to prove that the best empirical correlation for our results is the one given by Eq. 19.

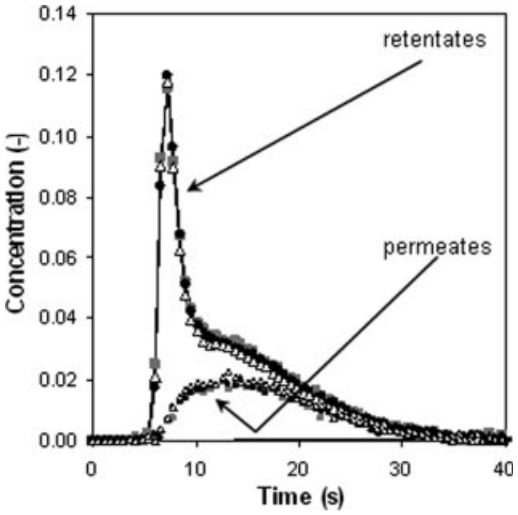

Figure 10. Example of outlet normal butane concentration evolutions (membrane: M1, temperature: 200°C, volumetric inner and outer compartment flow rates: 1.48 cm^3 s^{-1}) for different Dirac-like injections, ■: 8.8 μmol; ●: 1.1 μmol; △: 1.3 μmol.

Butane Isomers Sorption and Diffusion in the Zeolite Selective Layer

Once the mean selective layer thickness e_z is known, the hydrocarbon adsorption equilibrium constant and diffusivity can be calculated from the estimated values of τ_z and B_z, according to the relations: $D_z = e_z^2/\tau_z$ and $\kappa_A = B_z e_z/D_z$.

A graphical verification of the experiments linearity has been performed. For example, the Figure 10 is a result obtained for normal butane. The normalized retentate and permeate responses to three different concentration pulse intensities (respectively 8.8 μmol, 11 μmol, and 13 μmol) superimpose themselves perfectly. This observation means that the tests were realized within the linear response domain of the membrane. Consequently, the permeation parameters can be assumed to be constant.

Transient permeation experiments were realized on the membrane M1 at 200°C. Eight different flow rates between 0.5 and 3.5 cm^3 s^{-1} were tested to verify that the estimated parameters are not sensitive to the gases flow rates. An example of time domain fitting is presented on Figure 11.

The normal butane parameters estimated for the three membranes at 200°C are given in the Table 1. To be compared

Table 1. Equilibrium Constant and Diffusion Coefficient Obtained for Three Membranes at 200°C

Gaz	Membrane	M1	M2	M3
n-C_4	K_a (m^3_{gas} $m^{-3}_{zeolite}$)	71 ± 5	112	84
	$D_z \times 10^{10}$ (m^2. s^{-1})	3.5 ± 0.3	2.6	3.8
i-C_4	K_a (m^3_{gas} $m^{-3}_{zeolite}$)	–	49	40
	$D_z \times 10^{11}$ (m^2 s^{-1})	–	5.2	5.7

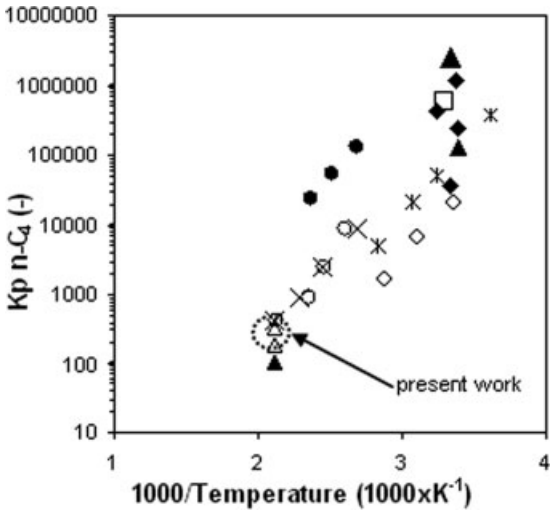

Figure 12. Comparison of the normal butane adsorption constant that we have obtained with the literature data.

◆ MFI[24]; ○ silicalite powder[24]; ▲ silicalite-1 (MFI)[46]; × silicalite-1 crystals[47]; ✱ silicalite-1[48]; ◇ silicalite-1[49]; ◆ MFI-silicalite type[50]; ▲ silicalite[5]; □ MFI zeolite membrane[51]; △ present work.

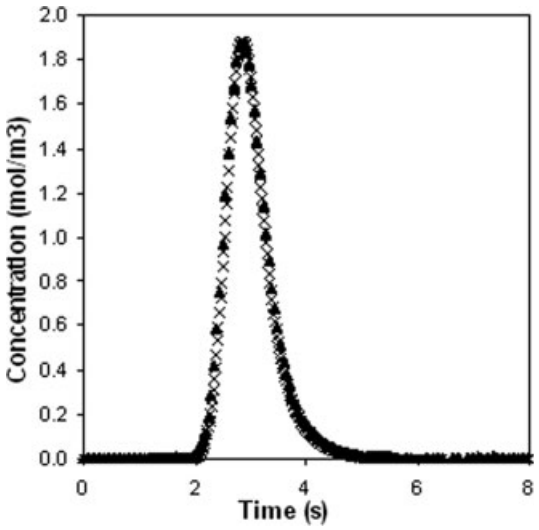

Figure 14. Example of outlet isobutane concentration evolutions (temperature 200°C, volumetric inner and outer compartment flow rates: 3.0 $cm^3\ s^{-1}$).

▲: membrane M1, ×: stainless steel tube.

with literature results (Figure 12), the adsorption coefficient κ_A of our pore-plugged membrane was corrected as follows:

$$K_A = \frac{\kappa_A}{1-\varepsilon} \tag{20}$$

One can notice that the diffusion and adsorption coefficients of normal butane in the membranes M1, M2, and M3 are very close. Contrary to the significant influence of the synthesis procedure on the zeolite membrane effective thickness, no sensitive influence on the physico–chemical properties has been thus observed.

The diffusion coefficient values that we have obtained are compared on Figure 13 with literature data. They are close to pulse field gradient nuclear magnetic resonance results of Heink et al.[52] They can also be favorably compared to the

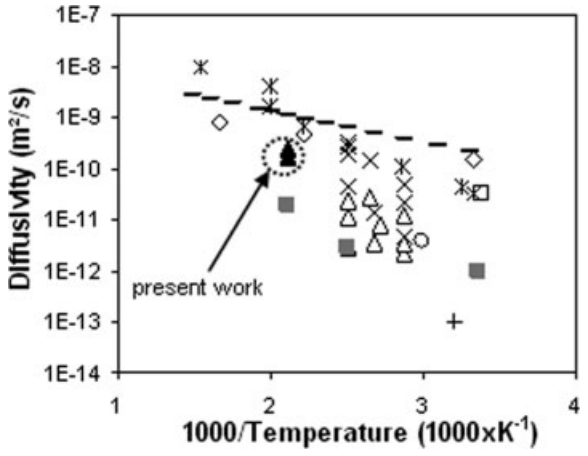

Figure 13. Comparison of the normal butane diffusion coefficient constant that we have obtained with the literature data.

□ silicalite membrane (membrane permeation)[35]; ◇ MFI-type zeolite (PFG-NMR)[52]; △ silicalite crystals (ZLC-Long-time)[6]; × silicalite crystals (ZLC-Short-time)[6]; ✱ membrane silicalite (MS and membrane permeation)[46]; ▬ ZSM-5 membrane (membrane permeation)[53]; ○ single silicalite crystal membrane (time lag)[54]; + MFI-zeolite membrane (Gas permeation and ZLC)[55]; ■ MFI silicalite-1 membrane (membrane permeation)[56].

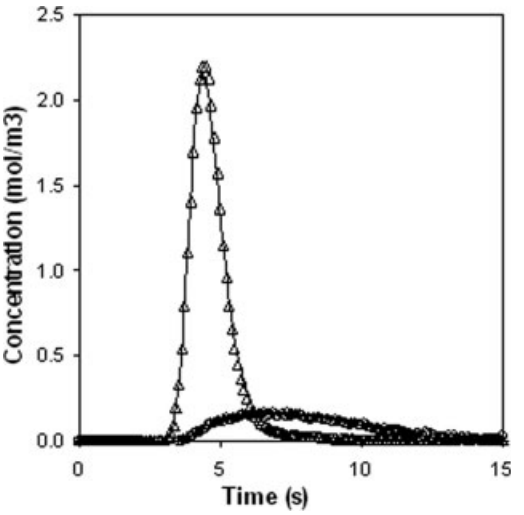

Figure 15. Example of outlet isobutane concentration evolutions (membrane: M3, temperature 200°C, volumetric inner and outer compartment flow rates: 3.0 $cm^3\ s^{-1}$).

Solid lines: model simulation; △: experimental values for the inner compartment, ○: experimental values for the outer compartment.

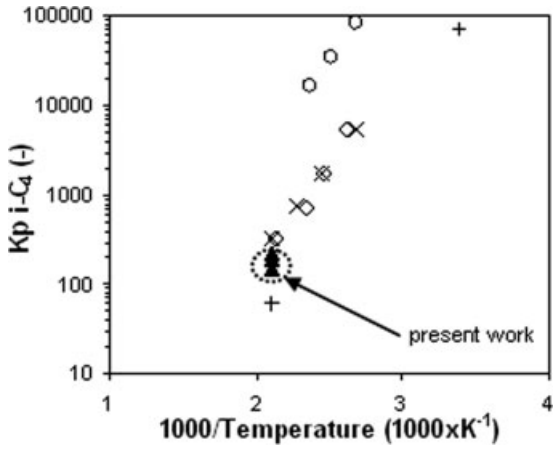

Figure 16. Comparison of the isobutane adsorption constant that we have obtained with the literature data.

◇ silicalite powder[24]; × silicalite-1 crystals[47]; ○ MFI-silicalite type[50]; + silicalite[5]; ▲ present work.

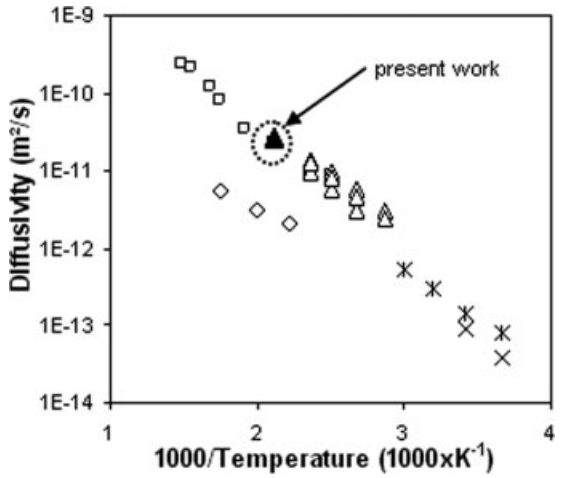

Figure 17. Comparison of the isobutane diffusion coefficient constant that we have obtained with the literature data.

□ ZSM-5 supported membranes (membrane permeation)[57]; ◇ ZSM-5 zeolite (QENS)[57]; △ silicalite crystals[6]; × MFI membrane (membrane permeation)[55]; ✱ ZSM-5 crystals (ZLC)[55].

Maxwell-Stefan diffusion coefficient found by Kapteijn et al.[46]

Isobutane transport parameters could not be obtained for the membrane M1. Its resistance to mass transport was too high to lead to a sensitive permeate response. As a consequence, the inner compartment response superimposed itself perfectly with the response obtained with the stainless steel tube (Figure 14). On the contrary, the M2 and M3 membranes are thin enough for the isobutane to cross the selective layer and permeate responses to be correctly detected. An example of model fitting obtained for the membrane M3 is presented on Figure 15.

The estimations that we have obtained for the isobutane Henry constant and diffusivity at 200°C are compared with literature data on Figures 16 and 17. One can see that our results are in good accordance with the published results.[5,23]

Finally, the large difference obtained between *n*-butane and isobutane diffusivities tends to prove that the zeolite membranes synthesized at IFP are well suited for paraffin's isomers separations.

Conclusion

A new transient permeation-based technique was proposed in the present article for the nondestructive *in-situ* physico–chemical and morphological characterization of zeolite composite membranes. This technique is based on the dynamic permeation experiments realized in the membrane linear response domain coupled with a parameter estimation procedure. The main advantage of such a transient state method is its experimental simplicity enabling the fast characterization of numerous membranes samples.

From a structural analysis of the model, we propose a step-by-step procedure for the parameters estimations. This approach has been applied and some preliminary results have been obtained for the thicknesses, transport, and equilibrium properties of butane isomers within MFI layers. Our results are favorably compared to the literature data and the method has been validated for hydrocarbons permeating in the Henry domain. An extension of the method to the transport properties determination at high concentrations is expected in the very next future. We also plan to extend our approach to mixtures.

Notation

$A(s)$, $a_1(s)$, $a_2(s)$ = transfer functions involved in the structural identifiability study
a = interfacial surface area, m^{-1}
$B(s)$, $C(s)$ = transfer functions involved in the structural identifiability study
$B_z = \frac{\kappa_A D_z}{e_z}$ = mass transfer parameter, m s^{-1}
C, $\hat{C}$ = gas phase concentration and its Laplace transform, mol m^{-3}
d_H = hydraulic diameter, m
$D(s)$ = transfer function involved in the structural identifiability study
D_z = adsorbate diffusion coefficient in the zeolite layer, m^2 s^{-1}
D_m = molecular diffusion coefficient, m^2 s^{-1}
D_{ax} = gas phase dispersion coefficient, m^2 s^{-1}
e_z = zeolite layer effective thickness, m
$G(s)$, $H(s)$ = transfer functions involved in the structural identifiability study
k = mass transfer coefficients, m s^{-1}
K_A = adsorption equilibrium constant
l_o = transfer functions involved in the structural identifiability study
L_z = zeolite layer length, m
L_1, L_2, L_4, L_5 = lengths of the enameled sections and of the connection tubes, m
$L_{t,i}$, $L_{t,o}$ = total length of the plug-dispersed flows, m
$Pe^L = \frac{vL}{D_{ax}}$ = Peclet number with respect to L
q = adsorbate concentration in the zeolite layer, mol m^{-3}
q_{sat} = saturation adsorbate concentration in the zeolite layer, mol kg^{-1}
$Re = \frac{\rho v L}{\mu}$ = Reynolds number defined with respect to the axial length

$Re_{d_H} = \frac{\rho v d_H}{\mu}$ = Reynolds number defined with respect to the hydraulic diameter
R = ideal gas constant, J mol^{-1} K^{-1}
R_i = inner zeolithe layer radius, m
$r_1(s)$, $r_2(s)$ = transfer functions involved in the structural identifiability study
r = radial coordinate in the zeolite layer for the simplified model, m
$Sc = \frac{\mu}{D_m}$ = Schmidt number
$Sh = \frac{k_0 d_H}{D_m}$ = Sherwood number
s = Laplace variable, s^{-1}
T = temperature, K
v = gas phase velocity, m s^{-1}
z = axial coordinate along the tube, m
z_2, z_3 = axial coordinates corresponding to the zone containing the zeolite layer, m
z_1 = axial coordinate corresponding to the CSTR outlet, m
z_4, z_5 = axial coordinates corresponding to the inner and outer compartments outlet dead volumes, m
t = time, s
V^{CSTR} = volume of a CSTR element, m^3

Greek letters

ε = support porosity
κ_A = equilibrium constant of the model $\kappa_A = K_A (1 - \varepsilon$
$\xi = \frac{z_3 - z_2}{L_z}$, $\xi_2 = \frac{z_2 - z_1}{L_1}$, $\xi_4 = \frac{z_4 - z_3}{L_4}$, $\xi_5 = \frac{z_5 - z_3}{L_5}$ = dimensionless axial coordinates
$\eta = \frac{r - R_i}{e_z}$ = dimensionless radial coordinate in the zeolite layer
$\tau^L = \frac{L}{v}$ = time constant in a gas phase plug—axial dispersed flow, s
τ^{CSTR} = mean residence time in a CSTR, s
$\tau_z = \frac{e_z^2}{D_z}$ = diffusion time constant, s
μ = gas phase viscosity, m^2 s^{-1}
ρ = mass density, kg m^{-3}
α, $\phi(\alpha)$ = variables involved in Eq. 18
$\Delta(s)$ = transfer function involved in the structural identifiability study

Subscripts

i = inner compartment
o = outer compartment
s = macroporous support
z = zeolite layer

Superscripts

* = a gas phase at equilibrium with a given solid
$i - C_4$ = related to isobutane
$n - C_4$ = related to normal butane

Literature Cited

1. Jallut C, Thomas G, Touré Y, Diard JP. Estimation de paramètres physico-chimiques et problèmes inverses. In: Corriou JP, editor. *Automatique Et Procédés Chimiques*. Paris: Hermes Science, 2001:51–99.
2. Gembarovic J, Vozar L, Majernik V. Using the least square method for data reduction in the flash method. *Int J Heat Mass Transfer*. 1990;33:1563–1565.
3. Roetzel W, Luo X, Xuan Y. Measurement of heat transfer coefficient and axial dispersion coefficient using temperature oscillations. *Exp Therm Fluid Sci*. 1993;7:345–353.
4. Ros S, Jallut C, Grillot JM, Amblard M. A transient-state technique for the heat transfer coefficient measurement in a corrugated plate heat exchanger channel based on frequency response and residence time distribution. *Int J Heat Mass Transfer*. 1995;38:1317–1325.
5. Hufton JR, Danner RP. Chromatographic study of alkanes in silicalite: equilibrium properties. *AIChE J*. 1993;39:954–961.
6. Hufton JR, Danner RP. Chromatographic study of alkanes in silicalite: transport properties. *AIChE J*. 1993;39:962–974.
7. Jolimaitre E, Tayakout-Fayolle M, Jallut C, Ragil K. Determination of mass transfer and thermodynamic properties of branched paraffins in silicalite by inverse chromatography technique. *Ind Eng Chem Res*. 2001;40:914–926.
8. Vonmeien OF, Biscaia EC, Nobrega R. Polymer-solute diffusion and equilibrium parameters by inverse gas chromatography. *AIChE J*. 1997;43:2932–2943.
9. Fujasova M, Linek V, Moucha T. Mass transfer correlations for multiple-impeller gas-liquid contactors. Analysis of the effect of axial dispersion in gas and liquid phases on 'local' kLa values measured by the dynamic pressure method in individual stages of the vessel. *Chem Eng Sci*. 2007;62:1650–1669.
10. Navarro-Laboulais J, Cardona SC, Torregrosa JI, Abad A, Lopez F. Structural identifiability analysis of the dynamic gas-liquid film model. *AIChE J*. 2006;52:2851–2863.
11. Perrin S, Chaudourne S, Jallut C, Lieto J. Transient state techniques for mass transfer characterization of a gas-liquid packed column. *Chem Eng Sci*. 2002;57:3335–3345.
12. Gleaves JT, Yablonskii GS, Phanawadee P, Schuurman Y. TAP-2: an interrogative kinetics approach. *Appl Catal A*. 1997;160:55–88.
13. Delgado JA, Nijhuis TA, Kapteijn F, Moulijn JA. Determination of adsorption and diffusion parameters in zeolites through a structured approach. *Chem Eng Sci*. 2004;59:2477–2487.
14. Berthier F, Diard JP, Montella C, Pronzato L, Walter E. Choice of experimental method induced by structural properties of mechanisms. *J Electroanal Chem*. 1995;399:1–6.
15. Kruczek B, Frisch HL, Chapanian R. Analytical solution for the effective time lag of a membrane in a permeate tube collector in which Knudsen flow regime exists. *J Membr Sci*. 2005;256:57–63.
16. Taveira P, Mendes A, Costa C. On the determination of diffusivity and sorption coefficients using different time-lag models. *J Membr Sci*. 2003;221:123–133.
17. Sanchez J, Gijiu CL, Hynek V, Muntean O, Julbe A. The application of transient time-lag method for the diffusion coefficient estimation on zeolite composite membranes. *Sep Purif Technol*. 2001;25:467–474.
18. Bennett KH, Cook KD, Falconer JL, Noble RD. Time-dependent permeance of gas mixtures through zeolite membranes. *Anal Chem*. 1999;71:1016–1020.
19. Gardner TQ, Falconer JL, Noble RD. Adsorption and diffusion properties of zeolite membranes by transient permeation. *Desalination*. 2002;149:435–440.
20. Walter E, Pronzato L. *Identification of Parametric Models from Experimental Data*. Berlin: Springer, 1997.
21. Couenne F, Jallut C, Tayakout-Fayolle M. On minimal representation of heterogeneous mass transfer for simulation and parameter estimation: application to breakthrough curves exploitation. *Comput Chem Eng*. 2005;30:42–53.
22. Tayakout-Fayolle M, Jolimaitre E, Jallut C. Consequence of structural identifiability properties on state-model formulation for linear inverse chromatography. *Chem Eng Sci*. 2000;55:2945–2956.
23. Gardner TQ, Flores AI, Noble RD, Falconer JL. Transient measurements of adsorption and diffusion in H-ZSM-5 membranes. *AIChE J*. 2002;48:1155–1167.
24. Gardner TQ, Lee JB, Noble RD, Falconer JL. Adsorption and diffusion properties of butanes in ZSM-5 zeolite membranes. *Ind Eng Chem Res*. 2002;41:4094–4105.
25. Chau C, Sicard M, Le Dred R. Membrane zéolithique de faible épaisseur, sa préparation et son utilisation en séparation. Eur. Pat. EP 1, 369,166 A1, 2003.
26. Chau C, Prevost I, Dalmon JA, Miachon S. Process for preparing supported zeolitic membranes by temperature-controlled crystallisation. U.S. Pat. 6,582,495 B2, 2003.
27. Chau C, Prevost I, Dalmon JA, Miachon S. Procédé de préparation de membranes zéolithiques supportées par cristallisation contrôlées en température. Eur. Pat. EP 1, 230,972 B1, 2006.
28. Wicke E, Kallenbach R. Die oberflächendiffusion von kohlendioxyd in aktiven kohlen. *Kolloid Z*. 1941;97:135–151.
29. Arnost D, Schneider P. Dynamic transport of multicomponent mixtures of gases in porous solids. *Chem Eng J Biochem Eng J*. 1995;57:91–99.

30. Biswasa J, Do DD, Greenfield PF, Smith JM. Evaluation of bidisperse transport properties of a reforming catalyst using a diffusion cell I. Theoretical development. *Appl Catal*. 1987;32: 217–234.
31. Biswasa J, Do DD, Greenfield PF, Smith JM. Evaluation of bidisperse transport properties of a reforming catalyst using a diffusion cell II. Experimental study. *Appl Catal*. 1987;32:235–247.
32. Burghardt A, Smith JM. Dynamic response of a single catalyst pellet. *Chem Eng Sci*. 1979;34:267–273.
33. Do DD, Smith JM. Transient response of diffusion cell containing a porous solid. *Chem Eng Sci*. 1984;39:1689–1699.
34. Dogu G, Smith JM. Rate parameters from dynamic experiments with single catalyst pellets. *Chem Eng Sci*. 1976;31:123–135.
35. Bakker WJW, Kapteijn F, Poppe J, Moulijn JA. Permeation characteristics of a metal-supported silicalite-1 zeolite membrane. *J Membr Sci*. 1996;117:57–78.
36. Sun MS, Talu O, Shah DB. Diffusion measurements through embedded zeolite cristal. *AIChE J*. 1996;42:3001–3007.
37. Courthial L, Baudot A, Jolimaitre E, Tayakout-Fayolle M, Jallut C. Moments method applied to the in-situ characterisation of normal butane mass transfer in MFI zeolite membranes. *Desalination*. 2006;193:215–223.
38. Tayakout-Fayolle M, Jallut C, Lefevre F, Dalmon JA. Application of transient methods to measurements of mass transfer parameters in zeolitic membranes. ECCE1, First European Congress on Chemical Engineering, Florence, Italy, May 4–7, 1997, Vol. 2, 1209–1212.
39. Poling BP, Prausnitz JM, O'Connel JP. *The Properties of Gases and Liquids*, 5th ed. Boston: McGraw-Hill, 2001.
40. Aris R. On the dispersion of a solute in a fluid flowing through a tube. *Proc R Soc Lond A*. 1956;235:67–77.
41. Ciavarella P, Moueddeb H, Miachon S, Fiaty K, Dalmon JA. Experimental study and numerical simulation of hydrogen/isobutane permeation and separation using MFI-zeolite membrane reactor. *Catal Today*. 2000;56:253–264.
42. Vasenkov S, Karger J. Evidence for the existence of intracistalline transport barriers in MFI-type zeolites: a model constituency check using MC simulations. *Microporous Mesoporous Mater*. 2002;55: 139–145.
43. Bakker WJW, Van den Broeke LJP, Kapteijn F, Moulijn JA. Temperature dependence of one-component permeation through a silicalite-1 membrane. *AIChE J*. 1997;43:2203–2214.
44. Ghosh UK, Upadhyay SN. Mass transfer to newtonian and non-newtonian fluids in short annuli. *AIChE J*. 1985;31:1721–1724.
45. Grober H, Erk S, Tate GE. *Fundamentals of Heat Transfer*. New York: McGraw-Hill, 1961.
46. Kapteijn F, Bakker WJW, Zheng G, Moulijn JA. Temperature- and occupancy-dependent diffusion of n-butane through a silicalite-1 membrane. *Microporous Mater*. 1994;3:227–234.
47. Zhu W, Van de Graaf JM, Van den Broeke LJP, Kapteijn F, Moulijn JA. TEOM: a unique technique for measuring adsorption properties. Light alkanes in silicalite-1. *Ind Eng Chem Res*. 1998;37: 1934–1942.
48. Pascual P, Ungerer P, Tavitian B, Boutin A. Development of a transferable guest-host force field for adsorption of hydrocarbons in zeolites. II. Prediction of alkenes adsorption and alkane/alkene selectivity in silicalite. *J Phys Chem B*. 2004;108:393–398.
49. Shen D, Rees LVC. Adsorption and diffusion on n-butane and 2-butyne in silicalite-1. *Zeolites*. 1991;11:684–689.
50. Ferreira AFP, Mittelmeijer-Hazeleger MC, Bliek A. Adsorption and differential heats of adsorption of normal and iso-butane on zeolite MFI. *Microporous Mesoporous Mater*. 2006;91:47–52.
51. Krishna R, Baur R. Analytic solution of the Maxwell-Stefan equations for multicomponent permeation across a zeolite membrane. *Chem Eng J*. 2004;97:37–45.
52. Heink W, Karger J, Pfeifer H, Datema K, Nowak AK. High-temperatured pulse field gradient nuclear magnetic resonance self-diffusion measurements of alkanes in MFI-type zeolites. *J Chem Soc Faraday Trans*. 1992;88:2505–3809.
53. Millot B, Méthivier A, Jobic H, Moueddeb H, Dalmon JA. Permeation of linear and branched alkanes in ZSM-5 supported membranes. *Microporous Mesoporous Mater*. 2000;38:85–95.
54. Hayhurst DT, Paravar AR. Diffusion of C1 to C5 normal paraffins in silicalite. *Zeolites*. 1988;8:27–29.
55. Jiang M, Eic M, Miachon S, Dalmon JA, Kocirik M. Diffusion of n-butane, isobutane and ethane in a MFI-zeolite membrane investigated by gas permeation and ZLC measurements. *Sep Purif Technol*. 2001;25:287–295.
56. Keizer K, Burggraaf AJ, Vroon ZAEP, Verweij H. Two component permeation through thin zeolite MFI membranes. *J Membr Sci*. 1998; 147:159–172.
57. Millot B, Méthivier A, Jobic H, Moueddeb H, Bee M. Diffusion of isobutane in ZSM-5 zeolite: a comparison of quasi-elastic neutron scattering and supported membrane results. *J Phys Chem B*. 1999; 103:1096–1101.

Manuscript received Sept. 6, 2007, and revision received Jun. 6, 2008.